



Cite this: *Soft Matter*, 2020, 16, 6138

Received 27th February 2020,  
Accepted 18th May 2020

DOI: 10.1039/d0sm00350f

rsc.li/soft-matter-journal

## First passage of an active particle in the presence of passive crowders†

Animesh Biswas,<sup>‡</sup> J. M. Cruz,<sup>‡</sup> P. Parmananda and Dibyendu Das<sup>\*</sup>

We experimentally study the stochastic transport of a self-propelled camphor boat, driven by Marangoni forces, through a crowd of passive paper discs floating on water. We analyze the statistics of the first passage times of the active particle to travel from the center of a circular container to its boundary. While the mean times rise monotonically as a function of the covered area fraction  $\phi$  of the passive paper discs, their fluctuations show a non-monotonic behavior – being higher at low and high value of  $\phi$  compared to intermediate values. The reason is traced to an interplay of two distinct sources of fluctuations – one intrinsic to the dynamics, while the other due to the crowding.

### 1 Introduction

Active matter has been of immense interest in science and engineering.<sup>1–3</sup> The active particles consume energy and convert it into directed motion. They may form biological systems like bacteria,<sup>4,5</sup> insects,<sup>6</sup> animals,<sup>7</sup> or synthetic systems of self-propelled rod, discs,<sup>8,9</sup> light-induced active particles,<sup>10,11</sup> or chemically driven systems.<sup>12,13</sup>

The Marangoni effect,<sup>14,15</sup> due to the surface tension gradient, may give rise to a chemical drive for an active particle. In this work, we study such a chemically driven entity, namely a camphor boat<sup>16,17</sup> made of camphor infused paper.<sup>18</sup> Van der Mensbrugge first explained the motion in 1869,<sup>19</sup> and lately, extensive works have been done in experiment and theory.<sup>20–31</sup> When such a boat is placed on the water surface, a molecular layer of camphor spreads around the boat and reduces the surface tension around it. If the spread is isotropic, the surface tension gradient induced forces would also be isotropic and hence lead to no net motion. Yet in reality, often small fluctuations exist, which lead to unbalanced directed forces, and hence resultant self-propelled motion. Thus the symmetry breaking is often spontaneous. If the shape of the particle is not a perfect circle, it could also be a source of asymmetry. The study of a self-propelled camphor boat has shown a rich and fascinating variety of kinetics, namely, translational, rotational,<sup>20,21</sup> intermittent,<sup>22,30</sup> collective,<sup>23,24</sup> and jammed.<sup>25</sup>

In natural situations, active particles often have to move through crowded environments, for example, the transport of

motor proteins inside a cell,<sup>32</sup> the transport of parasites through blood,<sup>33</sup> or bacterial motion through a disordered medium.<sup>34</sup> Theoretical studies have looked at active particles in quenched disordered media,<sup>35,36</sup> a single active particle moving through an assembly of movable passive crowders,<sup>37</sup> and mixtures of passive and active particles.<sup>38,39</sup> Interactions of microswimmers with obstacles have also been studied experimentally.<sup>40,41</sup> In our study, we have considered a single active camphor boat moving through an environment of paper discs, which are movable passive crowders, within a finite domain. Thus the obstacles (or disorder) in our experiments are not quenched in space.

Earlier studies have been interested in anomalous diffusion,<sup>36,42</sup> trapping and capture in crowded environments.<sup>35,40,43,44</sup> Yet for stochastic transport, another interesting question is first passage,<sup>45,46</sup> *i.e.*, the event when a target is reached by the particle for the first time. Unlike the relaxation times related to auto-correlation functions, the first passage time depends on the full history of a process until termination.<sup>47</sup> First passage processes have been of interest in physics,<sup>46,48,49</sup> chemistry,<sup>50,51</sup> and biology.<sup>52–54</sup> Within a confined geometry, such as a Petri dish in our experiments, first passage times are expected to have a finite mean and characteristic values.<sup>55–57</sup> This is in contrast to open geometries, where the mean first passage times may be infinite.<sup>45</sup> The study of first passage in experimental self-propelled systems is relatively rare. Theoretical models for run-and-tumble and active Brownian particles have studied first passage properties.<sup>58–61</sup> In this work, we experimentally study the first passage time of a camphor boat, to start from the center of a Petri dish and reach its periphery (target radius) for the first time, in the presence of passive crowders. We show that the temporal statistics has an interesting dependence on the density of the crowders.

Indian Institute of Technology Bombay, Powai-400076, Mumbai, India.

E-mail: animeshiitb@gmail.com

† Electronic supplementary information (ESI) available: Supporting videos and figures. See DOI: 10.1039/d0sm00350f

‡ Present address: Facultad de Ciencias en Física y Matemáticas, Universidad Autónoma de Chiapas, Tuxtla Gutiérrez, Chiapas 29050, México.

## 2 Experimental setup and method

The schematic diagram in Fig. 1(a) shows the experimental setup. A glass Petri dish (Borosil) of inner-diameter 13.5 cm is kept on a mounted platform and filled with 200 ml of deionized water. A circular paper disc of diameter 0.5 cm is cut out from a white paper sheet (BILT Copy Power Paper – A4, 75 GSM) to prepare the active camphor boat. The disc is then dipped in a 1.0 M camphor/ethanol solution (camphor, laboratory grade; ethanol  $\geq 98\%$ ) and left in the air to dry for  $15 \pm 1$  minutes. The passive floaters are circular shaped paper discs of diameter 0.5 cm, cut out from a pink paper sheet of a different material (M 9, scrapbook, Sundaram<sup>®</sup>). We place the passive paper discs on the water surface randomly, 15 minutes prior to the release of the active camphor boat. The packing fraction  $\phi$  of the floaters is obtained by dividing their net area by the area of the Petri dish. The floaters fill up the circular space forming interesting 2-dimensional patterns depending on  $\phi$  due to the local clustering of paper discs driven by forces of surface tension.<sup>62,63</sup> Such spatial structures and their fractal dimensions have been studied in the literature, *e.g.* using glass beads.<sup>64</sup> We may say qualitatively that with increasing  $\phi$  the dimensions of the clusters seem to rise. In Fig. 3 (panel a), we see that at lower values like  $\phi = 0.11$ , they form short linear chains, while for higher packing fractions like  $\phi = 0.44$ , they cover the space more homogeneously. The camphor particle is carefully released at the geometric center of the Petri dish from the tip of a syringe. We make sure that no passive floaters initially overlap with each other or with the camphor boat. A video camera (GoPro Hero-4) is kept below the platform to record the motion of the camphor boat. The videos are recorded at a rate of 120 fps. The experiments are performed under ultraviolet (UV) light for better tracking of the active particle trajectory – only the white-colored active disc glows under UV light, while the pink-colored passive floaters do not. From the video recording, we obtain the first passage time  $t$  of the camphor boat to reach the boundary of the Petri dish  $r(t) = R$  for the first time (as shown schematically in Fig. 1(b)). The trajectories of the camphor boat (Fig. 3 (panels b and c)) are plotted by extracting the  $x$  and  $y$  coordinates of the

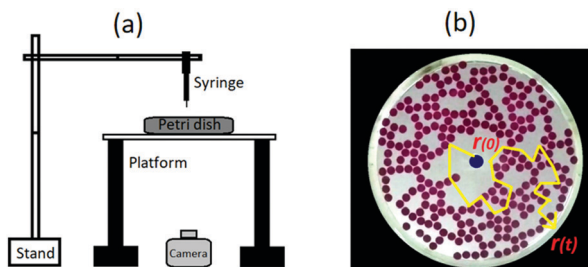


**Fig. 1** Schematic diagram of the experimental setup. (a) A Petri dish is kept on a mounted platform, and a camera is placed below it to record the motion of the camphor boat. The camphor boat is attached at the tip of a syringe needle and released initially at  $r = 0$ . (b) We show a schematic trajectory (yellow color) of the boat (blue color), which hits  $r(t) = R$  (radius of the Petri dish) at time  $t$  for the first time. The boat moves through a crowd of passive floaters (pink-colored paper discs) before reaching its target (which is the boundary of the dish).

boat in each video frame. For this, we use the MATLAB<sup>®</sup> interface (code developed by Blair and Dufresne,<sup>65</sup> which is based on the particle tracking algorithm of Crocker and Grier<sup>66</sup>). Throughout the experiments, the temperature is maintained at  $25 \pm 2$  °C.

We studied the system at different values of  $\phi$ , namely 0, 0.11, 0.18, 0.32, and 0.44. For every value of  $\phi$ , 100 experiments were performed, each time with fresh water, and with new passive and active floaters. Thus we obtained 100 different values of first passage times  $t$  for every  $\phi$ , which we use for statistical analysis. This was to ensure reasonably unbiased and adequate sampling within the experimental limitations.

From the literature of the stochastic processes, we know that the first passage is characterized by the first passage time distribution  $F(t)$ .<sup>45,47</sup> Apart from experimentally obtained  $F(t)$ , for our analysis, we use various other quantities related to it. We study the mean first passage time  $\langle t \rangle = \int_0^\infty F(t)t dt$ , and fluctuations as described by the Fano factor  $F_n = \frac{\text{Var}[t]}{\langle t \rangle}$ , where

$\text{Var}[t]$  is the variance. The behavior of  $F_n$  seen in our experiments suggests further careful study of fluctuations. Various recent studies in confined geometries<sup>57,67,68</sup> have found that when there is a large trajectory to trajectory variation in time scales, a good quantity to study is the distribution  $P(\omega)$  of the uniformity index  $\omega$ . Supposing  $t_1$  and  $t_2$  are two random first passage times, the stochastic variable  $\omega$  is defined as  $\omega = \frac{t_1}{t_1 + t_2}$ . When  $t_1$  and  $t_2$  are very different,  $\omega$  will be close to either 0 or 1. On the other hand,

if  $t_1$  and  $t_2$  are typically similar,  $\omega$  is close to  $\frac{1}{2}$ . Thus, the probability  $P(\omega)$  will be unimodal with a peak around  $\frac{1}{2}$  when

fluctuations in first passage times are low. In contrast, for large fluctuations in the values of  $t$ ,  $P(\omega)$  is expected to get broader and develop peaks near 0 and 1. Note that  $P(\omega)$  is formally related to

$$F(t) \text{ as } P(\omega) = \int_0^\infty \int_0^\infty \delta\left(\omega - \frac{t_1}{t_1 + t_2}\right) F(t_1)F(t_2) dt_1 dt_2.$$

In the following, we present the results for the statistics of first passage times and specifically highlight the non-monotonic behavior of fluctuations with increasing crowding of passive floaters. Through the analysis of representative trajectories of the active particle, we discuss the underlying causes for this behavior.

## 3 Results

The passive floaters are not fixed in space and can move around when pushed aside by the active particle. Yet with an increase in  $\phi$ , it is expected that they will increasingly obstruct the passage of the active particle from the center to the boundary. We see in Fig. 2(a) that this expectation is borne out – the mean first passage time  $\langle t \rangle$  monotonically rises with  $\phi$  as it is varied from 0 to 0.44. We see that an exponential functional form may fit the data over this limited range. Yet that cannot continue indefinitely, as  $\langle t \rangle$  is expected to diverge at a finite critical packing fraction, just like relaxation time does in a system approaching a jamming state.<sup>69</sup> The crowder densities in our

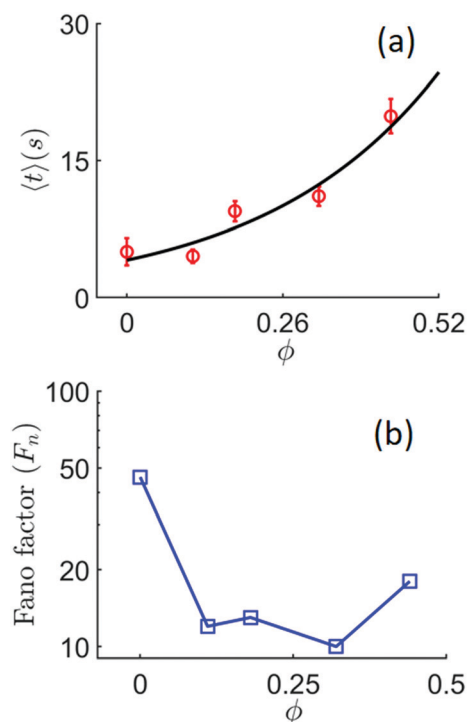


Fig. 2 (a) Mean first passage time  $\langle t \rangle$  as a function of  $\phi$  is seen to be monotonic. A curve  $\langle t \rangle \sim \exp(3.45\phi)$  is fitted. Standard errors are indicated by error bars. (b) Fano factor  $F_n$  as a function of  $\phi$  shows a non-monotonic behavior.

experiments are far from that of the jammed state, and hence very slow dynamics is not expected.

In Fig. 2(b), we show the Fano factor  $F_n$ , which measures the fluctuations in the first passage times. We see an interesting non-monotonic behavior of  $F_n$ . It is high at low  $\phi$ , then passes through a minimum at intermediate  $\phi$  (around 0.32), and finally rises again beyond  $\phi = 0.32$ . The existence of an optimal packing density  $\phi$  indicated by the non-monotonicity of fluctuations is an interesting feature, and the results that follow delve into its origin. We will see that passive particles serve as both suppressors of certain fluctuations and initiators of others, controlling the point of optimality. High fluctuations indicate that the first passage times are rather dissimilar from each other at both low and high values of  $\phi$ . We would show below that the reason for this large variability is distinct in the two regimes. When fluctuations are high, the mean value  $\langle t \rangle$  is not an adequate representative of the stochastic time scales. We need to look at the full distribution  $F(t)$  of the times  $t$ , as well as other measures of fluctuation. We do this below for the three regimes of  $\phi$  (low, intermediate, and high), along with analysis of the actual trajectories which explains the temporal variability.

(i) Low  $\phi$ : At the lowest packing fraction  $\phi = 0$ , where there are no passive obstacles, the distribution  $F(t)$  versus  $t$  is shown in Fig. 3 (panel d). It has an initial exponential decay over a short typical time  $\sim 2$  s, indicating that a fraction of the observed trajectories are short, and the particle quickly reaches from the center to the boundary. One such trajectory is shown in Fig. 3 (panel b) for  $\phi = 0$ . Yet, in the same figure (Fig. 3 (panel d)),

we see that a significant fraction of time scales are much larger ( $t \sim 50 - 100$  s). Why do such long time scales arise? In Fig. 3 (panel c), we show a representative long trajectory, where the active particle moves in successive incomplete circles of radii smaller than the Petri dish radius  $R$ , repeatedly, until it hits the boundary for the first time. A video MOV1 may be seen in the ESI.† It is apparent that the active camphor boat has an inherent angular motion, as known from earlier experiments.<sup>20,21,70</sup> Additionally, an interplay with the ambient noise causes the radii of the circular segments of the trajectory to vary stochastically. As a result, sometimes, the trajectory radius is initially large, and the boat reaches the boundary quickly, while at other times, circles of smaller radii repeatedly occur, leading to long first passage time. The oscillatory motion of the  $x$ -coordinate of the particle for a long trajectory is shown in Fig. 4(a). In Fig. 3 (panel e) we see the plot of  $P(\omega)$  which has peaks at  $\omega = 0, 1$ , and  $\frac{1}{2}$ . As discussed above, the peaks at  $\omega = 0$ , and 1 are indicative of random pairs of timescales being very different (corresponding to one short and another long trajectory). The peak at  $\omega = \frac{1}{2}$  corresponds to random pairs of trajectories, which are both long or both short.

At low  $\phi \neq 0$ , namely  $\phi = 0.11$ , the passive floaters start to obstruct the inherent roughly circular motion of the active particle. Thus the extremely long trajectories (as in the case of  $\phi = 0$ ) start getting eliminated. Yet, the scenario is not yet very different from  $\phi = 0$ . In Fig. 3 (panel d), we see that for  $\phi = 0.11$ ,  $F(t)$  has an initial exponential decay over  $\sim 4$  s, but it also has weightage at longer timescales ( $t \sim 25 - 40$  s). In Fig. 3 (panel b) we see that the number and size of the circular loops are reduced. A video MOV2 may be seen in ESI.† Some long trajectories (like the one in Fig. 3 (panel c)) stay quite distinct and discernable from the majority. As a consequence, in Fig. 3 (panel e),  $P(\omega)$  stays broad with peaks (although smaller in height) near 0 and 1, away from  $\omega = \frac{1}{2}$ .

In summary, for the low  $\phi$  regime, the inherent (noisy) circular motion of the active particle within the finite domain of the disc gives rise to some long and many short trajectories. The passive floaters intervene in the process and cut down some of the long sojourns. Yet the fluctuations stay strong, which is reflected in the high value of  $F_n$ , presence of multiple timescales in  $F(t)$ , and multimodality in  $P(\omega)$ .

(ii) Intermediate  $\phi$ : As the density of the passive floaters rises, for instance, in the case  $\phi = 0.32$ , we see from Fig. 3 (panel d) that  $F(t)$  becomes a more clearer exponential decay with a characteristic time  $\sim 9$  s. The instances of long trajectories are very rare. See a representative video MOV3 in ESI.† In Fig. 3 (panels b and c), we find that the length of the “shorter” and “longer” trajectories is not much different. This is clearly captured through the distribution  $P(\omega)$ . It is now seen (Fig. 3 (panel e)) to be unimodal, with a peak around  $\omega = \frac{1}{2}$ . This is consistent with the comparatively lower value of  $F_n$  (Fig. 2(b)) for this case.

(iii) High  $\phi$ : As  $\phi$  is further raised, the passive discs create more jamming. For  $\phi = 0.44$ , we see that although  $F(t)$  (Fig. 3 (panel d)) has a typical decay over  $\sim 15$  s, there are a sizeable number of outliers with longer timescales ( $t \sim 60-100$  s). Thus

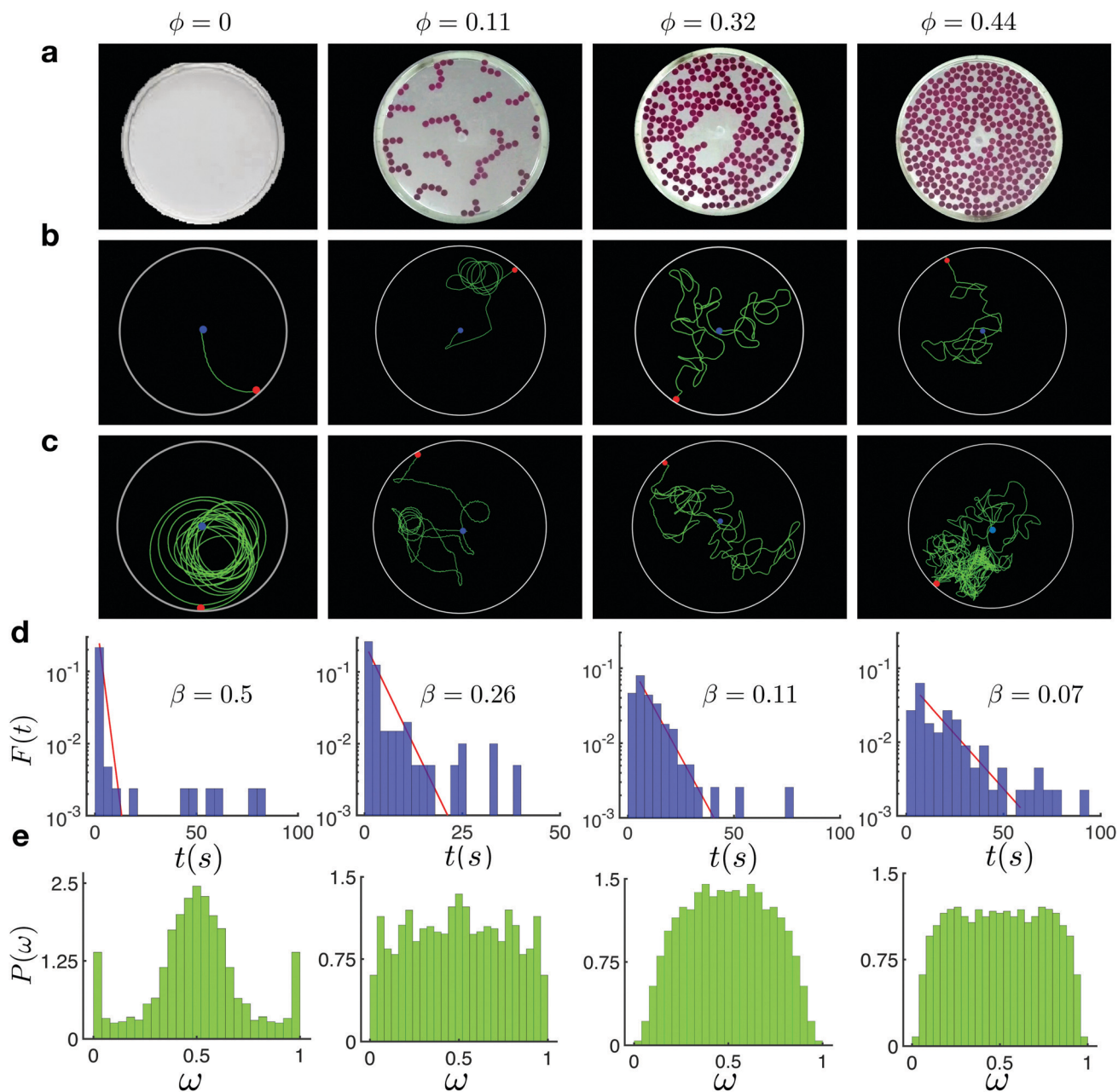


**Fig. 3** Spatial configurations of the passive crowders (panel a), short (panel b) and long (panel c) trajectories of the active particle, first passage time distribution  $F(t)$  (panel d) and uniformity index distribution  $P(\omega)$  (panel e) are shown for different values of  $\phi$ : 0, 0.11, 0.32, and 0.44, respectively. For  $\phi = 0$ , in panels b and c, noisy circular loops are visible. In contrast, for  $\phi = 0.44$ , the trajectory (in panel c) resembles a random motion. In panel d, for low and high  $\phi$ , we see a significant fraction of outliers with time  $t$ , which do not fall on the short time exponential fits.  $P(\omega)$  (in panel e) has a unimodal behavior for intermediate  $\phi = 0.32$ , but not for low and high  $\phi$ .

there are a fraction of long trajectories in addition to many short ones. The timescale diversity and hence high fluctuations in first passage times resemble the case of low densities like  $\phi = 0$  and differ from the intermediate  $\phi$  discussed above.  $P(\omega)$  becomes broad and develops “shoulders” away from  $\omega = \frac{1}{2}$  and towards  $\omega = 0$  and 1 (see Fig. 3 (panel e) for  $\phi = 0.44$ ).

On the other hand, a look at the representative short and long trajectories shown in Fig. 3 (panels b and c) reveals that those of  $\phi = 0.44$  are significantly different from those of  $\phi = 0$ .

There are no circular loops in the former case. A video MOV4 may be seen in ESI.† We understand that this regime is controlled by the locally dense passive floaters. The active particle moves from one temporary local trap to another, formed by the obstacles, and the resultant motion is random on the 2-d surface (see Fig. 3 (panel c)). In Fig. 4(a) and (b), the time evolution of the  $x$ -position of the particle for the two cases is compared – for  $\phi = 0$  the position has some oscillations, while for  $\phi = 0.44$  it seems diffusive. A useful quantity is the distribution of displacements  $\Delta x$  of the particle, for a given

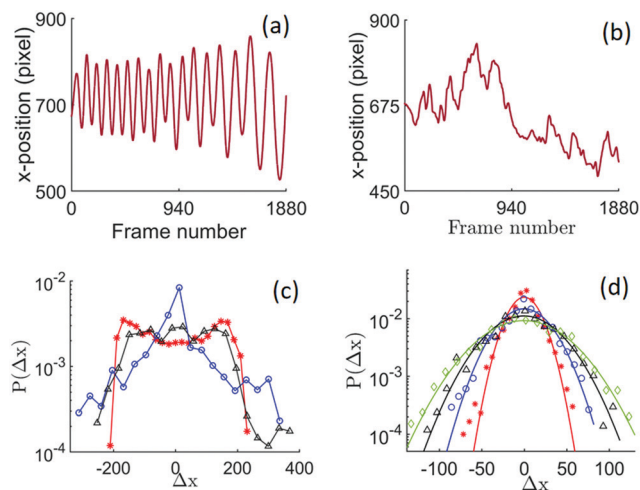


**Fig. 4** Time evolution of the  $x$ -position of a camphor boat for (a)  $\phi = 0$  and (b)  $\phi = 0.44$ . The oscillatory behaviour in (a) is different from the random behaviour in (b). Displacement distributions  $P(\Delta x)$  against displacement  $\Delta x$  (in units of pixel = 0.26 mm), at different chosen time intervals  $\Delta t$  (in units of frame number), for  $\phi = 0$  and 0.44 in (c) and (d), respectively. In (c), for  $\phi = 0$ : the distribution at  $\Delta t = 40$  (\*, red) is bimodal, at  $\Delta t = 90$  (○, blue) is unimodal, and at  $\Delta t = 140$  (△, black) is bimodal again. In (d), for  $\phi = 0.44$ : distributions are shown with respective Gaussian fits for intervals  $\Delta t = 15$  (\*, red),  $\Delta t = 30$  (○, blue),  $\Delta t = 60$  (△, black), and  $\Delta t = 90$  (◇, green).

time interval  $\Delta t$ . In Fig. 4(d), we see that for  $\phi = 0.44$ , they have Gaussian forms with widths increasing as  $\sim \Delta t^2$ . A data collapse of these curves with  $\alpha = 0.5$  is shown in Fig. S1 in ESI,<sup>†</sup> which implies ordinary diffusion. The data for the mean square displacement  $\langle (\Delta x)^2 \rangle$  versus  $\Delta t$  (Fig. S2 in ESI<sup>†</sup>) show a ballistic behavior at small times, crossing over to the diffusive behavior just discussed, at larger times beyond  $\Delta t = \tau \approx 12$  frames (or 0.1 s). This time  $\tau$  is roughly the average time of passage of the active particle between encounters with the paper discs. In sharp contrast to high packing density, for  $\phi = 0$ , the distribution alternates between bimodal and unimodal forms periodically (see Fig. 4(c)) reflecting the underlying periodicity of the trajectories. Thus we would stress that though both low and high  $\phi$  have similar large fluctuations in first passage times, the mechanism by which long delays arise in the high  $\phi$  regime is entirely different from that in the low  $\phi$  regime.

## 4 Discussion

In the biological context of living cells, active components often have to move from one part of the cell to another. They have to move amidst many other passive and active cellular components.<sup>32</sup> Often reaching a target zone for the first time may be of interest. Motivated by such general situations, we have done experiments on a simple representative physico-chemical<sup>71</sup> system. We study a chemically active camphor particle which travels through a crowd of passive paper discs, and we characterise the statistics of stochastic times involved in the process of transport from the center to the periphery of a confined region. The fields of ‘active transport’ and ‘first passage’ are both of contemporary interest; this work is an instance which combines the two. As noted in the

introduction, the first passage of active particles has received recent theoretical attention, while experiments on this topic were lacking.

Due to the size of the active particle (0.5 cm diameter), its thermal diffusivity is negligible at room temperature. In the literature, self-propelled motion has often been modelled by Active Brownian particles and Run-and-tumble particles<sup>72</sup> – but these cannot describe the two-dimensional motion of a camphor boat which has a deterministic component of circular motion, reminiscent of the motion of microtubules propelled by surface-bound dynein motors.<sup>73</sup> Apart from the viscous drag, the motion of a camphor particle is chiefly driven by the force proportional to the gradient of surface tension  $\nabla\gamma$ , where the surface tension  $\gamma(c(x(t),y(t),t))$  depends on the local concentration  $c$  of camphor which varies over space and time.<sup>74</sup> The stochastic dissolution of the camphor molecules from the active disc into water, their diffusive spreading, and their sublimation all contribute to make the evolution of  $c$  noisy. The angular and radial drive, along with this underlying noise, produce the approximate circular trails with a moving centre and varying radii. Once such a trajectory reaches the boundary of the dish, the first passage happens – so the finite radius of the vessel contributes to the values of the first passage times.

The inherently noisy circular motion of the active particle faces a second source of noise with the rise of the number of passive crowders in the system. Though movable, the crowders collectively present a spatial disorder, obstructing the passage of the camphor particle. This effect gets stronger with the growing crowder density  $\phi$ , and the inherent complex dynamics of the camphor boat gets replaced by random motion. It is known that an Active Brownian particle within a dense cluster of interacting active particles acquires a new effective anomalous dynamics different from its inherent dynamics in isolation.<sup>42</sup> In analogy we found that the new effective random motion of the camphor boat interacting with the crowders (at  $\phi = 0.44$ ) shows a short time ballistic and a large time diffusive behavior. Such motion has apparent resemblance to the motion of an isolated Active Brownian particle,<sup>75</sup> but whether there is a true equivalence of the two systems can only be confirmed from further studies in future. We hope that a computational model for this experiment would be built in future. It would need to introduce suitable effective active–passive and passive–passive interactions, and study the time evolution of the multi-particle system through simulations.

Optimal points are of general interest in the field of non-linear and stochastic systems. For example, one may recall that noise at the threshold of a bifurcation point of a non-linear system leads to the phenomenon of ‘Coherence resonance’ – the optimality of noise strength arising due to the competition of refractory periods and escape times.<sup>76</sup> Another example is ‘Stochastic resetting’ of random processes – this strategic regulation eliminates long trajectories, but also introduce new delays, leading to an optimal resetting rate where the mean first passage time is a minimum.<sup>77</sup> The system studied in this work also shows a similar point of optimality. The passive floaters suppress the inherent motion of the camphor particle and hence reduce the

fluctuations associated with that. Yet the crowding also introduces noise in the motion of the active particle, and thus enhances the fluctuations in transport. These competing tendencies lead to a novel effect – the fluctuations in first passage times attain a minimum at an optimal crowder density.

Future works may study the possibility of anomalous or slow glassy dynamics at packing densities not explored in this work. It would be also interesting to see how the results we have obtained depend on the shape of the passive crowders. For example, triangular, square, or cross-shaped<sup>37</sup> floaters may be studied. The active particle transport is more likely to get hindered if the edges of the passive particles are irregular. This work may also be extended in the future to study the first passage when two camphor boats come in close proximity (within a chosen radius) for the first time, in the presence of passive crowders. That problem would be one like a moving predator chasing a moving prey within a confined geometry and in the presence of obstacles.

## 5 Conclusion

We have experimentally studied the first passage transport of a self-propelled camphor boat through a crowd of paper discs, which serve as passive (movable) obstacles. As intuitively expected, the mean first passage time rises with the packing density  $\phi$  of the passive floaters. In contrast, the fluctuations of the first passage times vary in a non-monotonic way so as to lead to a point of optimality. In the low and high  $\phi$  regimes, fluctuations are high, albeit due to different physical reasons. On the other hand, around an intermediate  $\phi$  ( $\approx 0.32$ ), fluctuations are minimal – at these densities, timescales are more reliably predictable than at high and low  $\phi$ . The effect arises as the passive crowders eliminate a source of fluctuation while introducing a new one.

## Conflicts of interest

There are no conflicts to declare.

## Acknowledgements

The authors acknowledge financial support from IIT Bombay and DST India (project's reference no. EMR/2016/000275). We also thank members of our Nonlinear Dynamics and Statistical Physics Laboratory group for constructive discussions. D. D. would like to thank Amitabha Nandi and acknowledge SERB India (grant no. MTR/2019/000341) for financial support, and J. M. C. acknowledges CONACYT (Repatriación 2019-1).

## References

- 1 T. Vicsek and A. Zafeiris, *Phys. Rep.*, 2012, **517**, 71–140.
- 2 S. Ramaswamy, *Annu. Rev. Condens. Matter Phys.*, 2010, **1**, 323–345.
- 3 K. Han, C. W. Shields IV and O. D. Velev, *Adv. Funct. Mater.*, 2018, **28**, 1705953.
- 4 H.-P. Zhang, A. Be'er, E.-L. Florin and H. L. Swinney, *Proc. Natl. Acad. Sci. U. S. A.*, 2010, **107**, 13626–13630.
- 5 F. Peruani, J. Starruß, V. Jakovljevic, L. Søgaard-Andersen, A. Deutsch and M. Bär, *Phys. Rev. Lett.*, 2012, **108**, 098102.
- 6 J. Buhl, D. J. Sumpter, I. D. Couzin, J. J. Hale, E. Despland, E. R. Miller and S. J. Simpson, *Science*, 2006, **312**, 1402–1406.
- 7 K. Tunstrøm, Y. Katz, C. C. Ioannou, C. Huepe, M. J. Lutz and I. D. Couzin, *PLoS Comput. Biol.*, 2013, **9**, e1002915.
- 8 A. Kudrolli, G. Lumay, D. Volfson and L. S. Tsimring, *Phys. Rev. Lett.*, 2008, **100**, 058001.
- 9 J. Deseigne, O. Dauchot and H. Chaté, *Phys. Rev. Lett.*, 2010, **105**, 098001.
- 10 H.-R. Jiang, N. Yoshinaga and M. Sano, *Phys. Rev. Lett.*, 2010, **105**, 268302.
- 11 J. Palacci, S. Sacanna, A. P. Steinberg, D. J. Pine and P. M. Chaikin, *Science*, 2013, **339**, 936–940.
- 12 S. Thutupalli, R. Seemann and S. Herminghaus, *New J. Phys.*, 2011, **13**, 073021.
- 13 R. Kapral, *J. Chem. Phys.*, 2013, **138**, 020901.
- 14 L. Scriven and C. Sternling, *Nature*, 1960, **187**, 186–188.
- 15 P.-G. De Gennes, F. Brochard-Wyart and D. Quéré, *Capillarity and wetting phenomena: drops, bubbles, pearls, waves*, Springer Science & Business Media, 2013.
- 16 C. Tomlinson, *Proc. R. Soc. London*, 1862, 575–577.
- 17 L. Rayleigh, *Proc. R. Soc. London*, 1889, **47**, 364–367.
- 18 Y. S. Ikura, E. Heisler, A. Awazu, H. Nishimori and S. Nakata, *Phys. Rev. E*, 2013, **88**, 012911.
- 19 G. L. Van der Mensbrugge, *Sur la tension superficielle des liquides considérée au point de vue de certains mouvements observés à leur surface*, Hayez, 1869, vol. 1.
- 20 S. Nakata, Y. Iguchi, S. Ose, M. Kuboyama, T. Ishii and K. Yoshikawa, *Langmuir*, 1997, **13**, 4454–4458.
- 21 S. Nakata and Y. Hayashima, *J. Chem. Soc., Faraday Trans.*, 1998, **94**, 3655–3658.
- 22 N. J. Suematsu, Y. Ikura, M. Nagayama, H. Kitahata, N. Kawagishi, M. Murakami and S. Nakata, *J. Phys. Chem. C*, 2010, **114**, 9876–9882.
- 23 S. Soh, K. J. Bishop and B. A. Grzybowski, *J. Phys. Chem. B*, 2008, **112**, 10848–10853.
- 24 E. Heisler, N. J. Suematsu, A. Awazu and H. Nishimori, *J. Phys. Soc. Jpn.*, 2012, **81**, 074605.
- 25 H. Nishimori, N. J. Suematsu and S. Nakata, *J. Phys. Soc. Jpn.*, 2017, **86**, 101012.
- 26 N. J. Suematsu, T. Sasaki, S. Nakata and H. Kitahata, *Langmuir*, 2014, **30**, 8101–8108.
- 27 S. Nakata, M. Nagayama, H. Kitahata, N. J. Suematsu and T. Hasegawa, *Phys. Chem. Chem. Phys.*, 2015, **17**, 10326–10338.
- 28 Y. Koyano, M. Gryciuk, P. Skrobanska, M. Malecki, Y. Sumino, H. Kitahata and J. Gorecki, *Phys. Rev. E*, 2017, **96**, 012609.
- 29 K. Iida, H. Kitahata and M. Nagayama, *Phys. D*, 2014, **272**, 39–50.
- 30 V. Akella, D. K. Singh, S. Mandre and M. Bandi, *Phys. Lett. A*, 2018, **382**, 1176–1180.
- 31 J. Sharma, I. Tiwari, D. Das, P. Parmananda, V. Akella and V. Pimienta, *Phys. Rev. E*, 2019, **99**, 012204.

- 32 L. Conway, D. Wood, E. Tüzel and J. L. Ross, *Proc. Natl. Acad. Sci. U. S. A.*, 2012, **109**, 20814–20819.
- 33 N. Heddergott, T. Krüger, S. B. Babu, A. Wei, E. Stellamanns, S. Uppaluri, T. Pfohl, H. Stark and M. Engstler, *PLoS Pathog.*, 2012, **8**(11), e1003023.
- 34 J. E. Sosa-Hernández, M. Santillán and J. Santana-Solano, *Phys. Rev. E*, 2017, **95**, 032404.
- 35 F. Peruani and I. S. Aranson, *Phys. Rev. Lett.*, 2018, **120**, 238101.
- 36 O. Chepizhko and F. Peruani, *Phys. Rev. Lett.*, 2013, **111**, 160604.
- 37 R. Chatterjee, N. Segall, C. Merrigan, K. Ramola, B. Chakraborty and Y. Shokef, *J. Chem. Phys.*, 2019, **150**, 144508.
- 38 L. Wang and J. Simmchen, *Condens. Matter*, 2019, **4**, 78.
- 39 J. Stenhammar, R. Wittkowski, D. Marenduzzo and M. E. Cates, *Phys. Rev. Lett.*, 2015, **114**, 018301.
- 40 D. Takagi, J. Palacci, A. B. Braunschweig, M. J. Shelley and J. Zhang, *Soft Matter*, 2014, **10**, 1784–1789.
- 41 G. Volpe, I. Buttinoni, D. Vogt, H.-J. Kümmerer and C. Bechinger, *Soft Matter*, 2011, **7**, 8810–8815.
- 42 G. S. Redner, M. F. Hagan and A. Baskaran, *Phys. Rev. Lett.*, 2013, **110**, 055701.
- 43 A. Kaiser, K. Popowa, H. Wensink and H. Löwen, *Phys. Rev. E: Stat., Nonlinear, Soft Matter Phys.*, 2013, **88**, 022311.
- 44 S. E. Spagnolie, G. R. Moreno-Flores, D. Bartolo and E. Lauga, *Soft Matter*, 2015, **11**, 3396–3411.
- 45 S. Redner, *A guide to first-passage processes*, Cambridge University Press, 2001.
- 46 A. J. Bray, S. N. Majumdar and G. Schehr, *Adv. Phys.*, 2013, **62**, 225–361.
- 47 C. Gardiner, *et al.*, *Handbook of stochastic methods*, Springer, vol. 3, 1985.
- 48 J. Krug, H. Kallabis, S. Majumdar, S. Cornell, A. Bray and C. Sire, *Phys. Rev. E: Stat. Phys., Plasmas, Fluids, Relat. Interdiscip. Top.*, 1997, **56**, 2702.
- 49 D. Das and S. Sabhapandit, *Phys. Rev. Lett.*, 2008, **101**, 188301.
- 50 S. Reuveni, M. Urbakh and J. Klafter, *Proc. Natl. Acad. Sci. U. S. A.*, 2014, **111**, 4391–4396.
- 51 O. Bénichou, C. Chevalier, J. Klafter, B. Meyer and R. Voituriez, *Nat. Chem.*, 2010, **2**, 472.
- 52 T. Chou and M. R. D'Orsogna, in *First-passage phenomena and their applications*, World Scientific, 2014, pp. 306–345.
- 53 É. Roldán, A. Lisica, D. Sánchez-Taltavull and S. W. Grill, *Phys. Rev. E*, 2016, **93**, 062411.
- 54 J. J. Parmar, D. Das and R. Padinhateeri, *Nucleic Acids Res.*, 2015, **44**, 1630–1641.
- 55 A. Godec and R. Metzler, *Sci. Rep.*, 2016, **6**, 20349.
- 56 O. Bénichou and R. Voituriez, *Phys. Rep.*, 2014, **539**, 225–284.
- 57 I. Nayak, D. Das and A. Nandi, *Phys. Rev. Res.*, 2020, **2**, 013114.
- 58 L. Angelani, R. Di Leonardo and M. Paoluzzi, *Eur. Phys. J. E: Soft Matter Biol. Phys.*, 2014, **37**, 59.
- 59 K. Malakar, V. Jemseena, A. Kundu, K. V. Kumar, S. Sabhapandit, S. N. Majumdar, S. Redner and A. Dhar, *J. Stat. Mech.: Theory Exp.*, 2018, 043215.
- 60 A. Scacchi and A. Sharma, *Mol. Phys.*, 2018, **116**, 460–464.
- 61 U. Basu, S. N. Majumdar, A. Rosso and G. Schehr, *Phys. Rev. E*, 2018, **98**, 062121.
- 62 P. A. Kralchevsky and K. Nagayama, *Langmuir*, 1994, **10**, 23–36.
- 63 P. A. Kralchevsky and N. D. Denkov, *Curr. Opin. Colloid Interface Sci.*, 2001, **6**, 383–401.
- 64 Z. Hórvölgyi and M. Zrínyi, *Fractals*, 1993, **1**, 460–469.
- 65 D. Blair and E. Dufresne, Particle-tracking code available at <http://physics.georgetown.edu/matlab>, unpublished.
- 66 J. C. Crocker and D. G. Grier, *J. Colloid Interface Sci.*, 1996, **179**, 298–310.
- 67 T. G. Mattos, C. Mejía-Monasterio, R. Metzler and G. Oshanin, *Phys. Rev. E: Stat., Nonlinear, Soft Matter Phys.*, 2012, **86**, 031143.
- 68 C. Mejía-Monasterio, G. Oshanin and G. Schehr, *J. Stat. Mech.: Theory Exp.*, 2011, P06022.
- 69 P. Olsson, *Phys. Rev. Lett.*, 2019, **122**, 108003.
- 70 R. J. Löffler, M. M. Hanczyc and J. Gorecki, *Phys. Chem. Chem. Phys.*, 2019, **21**, 24852–24856.
- 71 S. Nakata, V. Pimienta, I. Lagzi, H. Kitahata and N. J. Suematsu, *Theoretical and Computational Chemistry Series: Physicochemical Design Based on Nonlinear Dynamics. Self-organized Motion*, Royal Society of Chemistry, 2018.
- 72 M. E. Cates and J. Tailleur, *EPL*, 2013, **101**, 20010.
- 73 Y. Sumino, K. H. Nagai, Y. Shitaka, D. Tanaka, K. Yoshikawa, H. Chaté and K. Oiwa, *Nature*, 2012, **483**, 448–452.
- 74 Y. Hayashima, M. Nagayama and S. Nakata, *J. Phys. Chem. B*, 2001, **105**, 5353–5357.
- 75 C. Bechinger, R. Di Leonardo, H. Löwen, C. Reichhardt, G. Volpe and G. Volpe, *Rev. Mod. Phys.*, 2016, **88**, 045006.
- 76 S. Biswas, D. Das, P. Parmananda and A. Sain, *Phys. Rev. E: Stat., Nonlinear, Soft Matter Phys.*, 2009, **80**, 046220.
- 77 M. R. Evans and S. N. Majumdar, *Phys. Rev. Lett.*, 2011, **106**, 160601.